Lab on a Chip

Accepted Manuscript

ROYAL SOCIETY OF CHEMISTRY

www.rsc.org/loc

Journal Name

ARTICLE TYPE

Cite this: DOI: 10.1039/xxxxxxxxxx

Microfabricated Reciprocating Micropump for Intracochlear Drug Delivery with Integrated Drug/Fluid Storage and Electronically Controlled Dosing

Vishal Tandon,[a,b*] Woo Seok Kang,[a*] Tremaan A. Robbins,[b] Abigail J. Spencer,[b] Ernest S. Kim,[b] Michael J. McKenna,[a] Sharon G. Kujawa,[a] Jason Fiering,[b] Erin E.L. Pararas,[b] Mark J. Mescher,[b] William F. Sewell,[a] and Jeffrey T. Borenstein[b]

Received Date
Accepted Date

DOI: 10.1039/xxxxxxxxxx

www.rsc.org/journalname

The anatomical and pharmacological inaccessibility of the inner ear is a major challenge in drug-based treatment of auditory disorders. This also makes pharmacokinetic characterization of new drugs with systemic delivery challenging, because efficacy is coupled with how efficiently a drug can reach its target. Direct delivery of drugs to cochlear fluids bypasses pharmacokinetic barriers and helps to minimize systemic toxicity, but anatomical barriers make administration of multiple doses difficult without an automated delivery system. Such a system may be required for hair-cell regeneration treatments, which will likely require timed delivery of several drugs. To address these challenges, we have developed a micropump for controlled, automated inner-ear drug delivery with the ultimate goal of producing a long-term implantable/wearable delivery system. The current pump is designed to be used with a head mount for guinea pigs in preclinical drug characterization experiments. In this system, we have addressed several microfluidic challenges, including maintaining controlled delivery at safe, low flow rates and delivering drug without increasing the volume of fluid in the cochlea. By integrating a drug reservoir and all fluidic components into the microfluidic structure of the pump, we have made the drug delivery system robust compared to previous systems that utilized separate, tubing-connected components. In this study, we characterized the pump's unique infuse-withdraw and on-demand dosing capabilities on the bench and in guinea pig animal models. For the animal experiments, we used DNQX, a glutamate receptor antagonist, as a physiological indicator of drug delivery. DNQX suppresses compound action potentials (CAPs), so we were able to infer the distribution and spreading of the DNQX over time by measuring the changes in CAPs in response to stimuli at several characteristic frequencies.

1 Introduction

One of the major bottlenecks in development of drug-based treatments for auditory disorders is that the inner ear is relatively inaccessible, both pharmacologically and anatomically. The presence of the blood-cochlear barrier limits access to the cochlea for many systemically delivered drugs.[1–3] This barrier can be bypassed by delivering drugs directly to the cochlear fluids, a process that also allows safe application of agents that might have detrimental systemic side effects.[4,5] However, the anatomic inaccessibility of the cochlea makes it difficult to physically administer multiple doses without the use of an automated delivery system.

An alternative to intracochlear delivery is to administer the

[a] *Department of Otology and Laryngology, Massachusetts Eye and Ear Infirmary and Harvard Medical School, 243 Charles Street, Boston, MA 02139, USA. E-mail: William_Sewell@meei.harvard.edu*

[b] *Materials Engineering and Microfabrication Directorate, Draper, 555 Technology Square, Cambridge, MA 02139, E-mail:jborenstein@draper.com.*

*Vishal Tandon and Woo Seok Kang are coauthors for this work.

drug into the middle ear and onto the round window membrane (RWM),[3,6] which can help to minimize systemic toxicity and intensify therapeutic efficacy. This delivery method, however, depends on drugs passively diffusing into the inner ear across the RWM, and the kinetics of this transport process are complex,[7] relatively slow, and can be unpredictable. As a result, the potential efficacy of RWM delivery for large, complex molecules or unstable drugs is suspect. Hence, many promising drug candidates may be incompatible with RWM delivery, including growth factor proteins,[8–11] siRNA and similar molecules,[12,13] and vectors for gene therapy,[14] further establishing the need for direct access to the inner ear via an automated intracochlear delivery system.

Such an automated delivery system requires stringent fluidic control because of the small volume of fluid (perilymph) that fills the cochlea and the high sensitivity of the auditory organ to mechanical displacement. Perilymph, an extracellular fluid similar in composition to cerebrospinal fluid, bathes the cellular structures of the cochlea and is the logical location for drug delivery in most cochlear targets. The human inner ear contains about 150–200 μL of perilymph,[15,16] of which only 50 μL reside in the scala tympani.[15,17] Studies in animals indicate that cochlear damage can be associated with prolonged intraochlear delivery at high flow rates.[18,19]

In addition to precise control of delivery volumes and flow rates, an automated system for intracochlear delivery must be sufficiently small and lightweight to be implanted near the cochlea (the mastoid bone is an ideal location;[20] a solution with an implantable portion and a wearable portion is acceptable) and robust enough to maintain consistent delivery of precise volumes of fluid in the submicroliter range over time periods ranging from days to months. For hair-cell regeneration applications, it will also be important that the system be configurable for delivery of a timed series of multiple agents,[21] regulated by a portable electronic control system, preferably one that enables remote activation/deactivation and real-time dosing changes.

There are currently no commercially available devices capable of meeting these requirements. Osmotic pumps are one example of a micropump that has been used commonly for preclinical experiments involving drug delivery via a cochleostomy.[22] Osmotic pumps, however, cannot be deactivated once infusion has started, and have limited payloads and lack precise flow control. The Round Window Microcatheter combined with a Panomat micropump was used clinically to deliver drug intratympanically over 4 weeks with mixed results,[23] but the system is too large for long term delivery, and is susceptible to the shortcomings of RWM delivery. Other commercial drug delivery pumps, including the Medtronic Synchromed (an active pump) and Isomed (a passive pump), are too large for mastoid implantation. General commercial micropumps, such as the Bartels Mikrotechnik MP6, can be assembled with other fluidic components into a functional delivery system.[24] However, as the number of components and fluidic connections between them increases, such systems become less robust. Delivery of multiple agents would require at least one pump per drug, so systems assembled using commercial pumps can become too large.

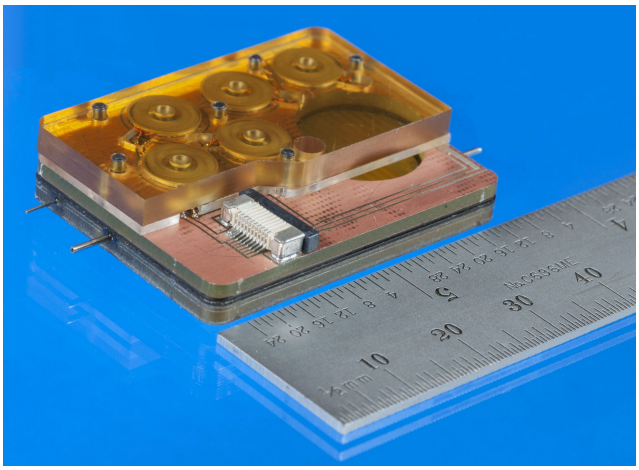

Fig. 1 Photograph of our reciprocating micropump comprising microfluidics, a printed circuit board (PCB), and 5 electromagnetic acutators with associated fixtures.

Here we describe the performance of a micropump with the capacity for automated drug delivery to the inner ear. We designed, fabricated, and characterized a reciprocating micropump that incorporates all of the essential microfluidic elements into a single, integrated structure (Figure 1). Like in our previous systems,[24–26] the pump is designed to be used in a head-mounted structure for long-term drug delivery experiments in guinea pig animal models with the ultimate goal of making it implantable in the human mastoid cavity. The micropump was fabricated by laminating several machined polymer layers together to form 3-D microfluidic structures, and then mounting miniature electromagnetic actuators to the fluidics to control valve and pumping action. The micropump has a fully integrated drug reservoir that is addressed by active valves, enabling electronically-controlled drug dosing and reciprocating delivery, making it suitable for use in preclinical drug characterization experiments. Integration of all fluidic components reduces the size and weight of the system toward the goal of producing an implantable device, and helps to make it robust for consistent delivery over long periods. A summary of micropumps reported in the literature to have been used for inner-ear drug delivery, along with capabilities added with new generations of pumps, is shown in Figure 2.

In designing this system, we also addressed several microfluidic challenges. Firstly, to keep the infused volume to a minimum, we employed a reciprocating delivery scheme,[18,21,24,25,27] where concentrated drug is infused into the scala tympani, allowed time

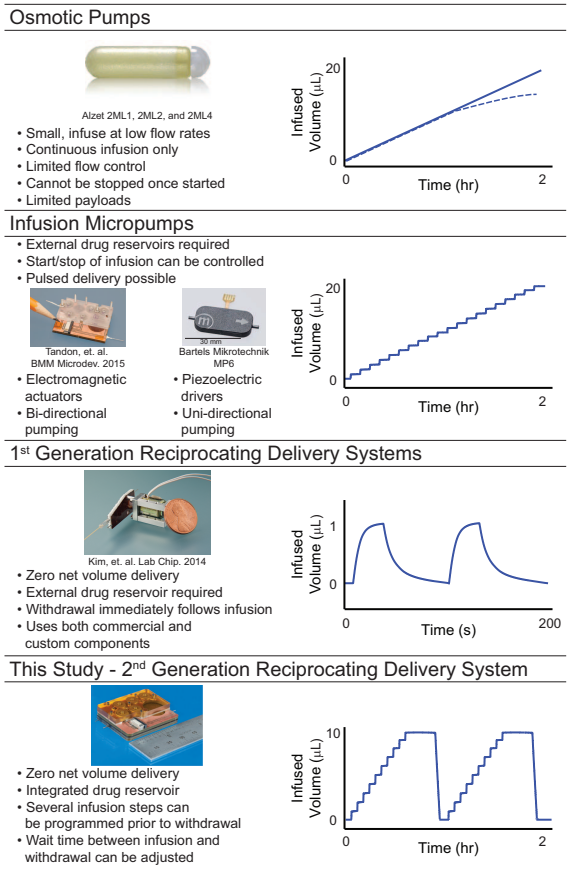

Fig. 2 Comparison of pump types including different generations of our inner-ear drug delivery systems. Representations of typical infusion profiles are shown on the right. For the osmotic pump, the dashed line indicates the possible decay in flow rate over time. For the first generation reciprocating delivery system, the time scale shown is much shorter (on the order of minutes as opposed to hours) because withdrawal of fluid in that system must immediately follow infusion, so the relevant time scale is that of individual pump strokes.

to diffuse, and then the infused fluid, now with a lower drug concentration, is withdrawn leading to net delivery with zero net volume increase of fluid in the cochlea. Secondly, we utilized hydrodynamic resistance and compliance to lower the instantaneous flow rates generated during delivery in order to reduce the possibility of mechanical damage to the inner ear associated with flow. Finally, we minimized dead volume in the system, particularly at the outlet of the pump, which helped to reduce the amount of pumping required to achieve delivery. This is critical for reciprocating delivery, and will also be important for future systems designed for delivery of multiple agents.

We chose target parameters for inner-ear drug delivery (e.g. flow rates, infusion volumes, and timing) based on our previous work in this area. We characterized our micropump in order to ensure that these targets were achieved and that the pump was functional in delivering drug to an animal model. However, as the underlying pumping technology driving this drug-delivery system is versatile, a full exploration of the potential of this technology is beyond the scope of this work. Here, we characterized the micropump by measuring both infuse and withdraw flow rates on the bench-top as a function of hydrodynamic resistance added to the outlet. On the bench, we loaded the drug reservoir with fluorescein solution and measured the fluorescence output of the pump after electronically activating drug dosing in order t demonstrate dose control.

We also demonstrated reciprocating inner-ear delivery and electronically-controlled dosing in the guinea pig, using the pump to infuse drug via a cochleostomy made at the basal turn. For this we loaded the drug reservoir with a glutamate receptor antagonist, DNQX, which disrupts hair-cell-to-auditory-nerve synaptic transmission resulting in attenuation of compound action potentials (CAPs) generated in response to auditory stimuli. As a control for nonspecific effects, we monitored the responses from hair cells—the distortion product otoacoustic emissions (DPOAEs)—which are not altered by DNQX. Both CAPs and DPOAEs can be elicited from specific regions along the ∼16-mm length of the cochlea, allowing us to monitor distribution of the drug during the infusions.

The development of a device to automate intracochlear delivery of agents could have a wide impact in treating hearing loss. Approximately 360 million people worldwide suffer from disabling hearing loss as estimated by the world health organization in 2012.[28] The most common form of hearing loss is sensorineural hearing loss (SNHL), in which damage to the sensory (hair) cells or auditory nerve impairs transduction or transmission of sound. While cochlear implants have been successful in restoring hearing capabilities to some patients with severe SNHL,[29] recent advances in the molecular biology of hearing[30–32] show promise for drug-based treatments for SNHL. Drug targets and potential therapeutic compounds have been identified for regeneration of hair cells and auditory nerve terminals, as well as protection from noise damage, ototoxic drugs (such as cisplatin and aminoglycosides), and adverse effects from radiation therapy.

2 Methods

2.1 System Overview

Many commercial membrane/diaphragm-based micropumps use check valves to achieve flow rectification, and are therefore limited to unidirectional flow between 2 ports, i.e., flow from a fluid reservoir connected to the inlet of the pump to tubing connected at the outlet (e.g., the Bartels Mikrotechnik MP6). More complex systems can be fabricated by combining several of these pumps, but only with additional fluidic connections (potential failure points), increased system size, and increased dead vol-

ume. Our micropump design employs electronically-controlled, individually-addressed, miniature electromagnetic actuators to control valve opening/closing and pump diaphragm displacement. Phased operation of the pump actuator with any two valve actuators results in net pumping of fluid from one valve to the other. This method of pumping supports bidirectional flow between the two ports, as well as the potential for microfluidic layouts for pumping between an arbitrary number of integrated pump chambers and ports, limited only by size, weight, and power consumption constraints for a given application.

We have designed and fabricated a micropump for inner-ear drug delivery that has 4 selectable ports (Figure 3). These ports are connected to: (i) a large fluidic capacitor used for fluid storage, C; (ii) an outlet that connects to the drug-delivery target, O; (iii) the outlet from an integrated drug reservoir, R1; (iv) the inlet to the integrated drug reservoir, R2. Each port is fluidically connected to a central pump chamber, and each is individually addressed with a valve. The valves are normally closed, meaning that no power is used when they are shut, and power must be supplied to their associated electromagnetic actuators in order to open them/hold them open. In order to minimize power consumption for future experiments in which the pump will be powered by a battery, we designed the microfluidics and chose the pump operating conditions so as to minimize the amount of time the valves are open.

The sequence of events for reciprocating drug delivery (Figure 4) is as follows: (i) an internal drug-refresh loop is run, transferring drug from the drug reservoir (ports R1 and R2) into the main infuse-withdraw line (between ports O and C); (ii) drug is infused into the cochlea (ports O and C) and some fluid is drained from the fluid storage capacitor; (iii) the first two steps can be repeated several times for additional doses; (iv) after the drug has been allowed to diffuse for some time, a volume of fluid is withdrawn from the cochlea (ports O and C) that is equal to the volume infused in steps (i)–(iii), refilling the fluid storage capacitor. This process results in net delivery of drug with zero net fluid volume added to the cochlea. Outlet dead volume and outlet resistance are critical design parameters in this delivery scheme (they are related to each other). Outlet dead volume (the summed volumes of the fluid spaces between the outlet valve and the cochlea, including any tubing attached to the pump) must be minimized in order to limit the amount of power used to transport fluid from the outlet of the pump to the cochlea. In a reciprocating delivery scheme, this dead volume will have to be cleared after every withdraw cycle. Outlet resistance reduces the flow rates generated by the pump. Resistance can be added to the outlet of the pump in order to reduce flow rates for safety, but this also adds dead volume and can potentially reduce power efficiency.

Fluidic capacitors adjacent to each valve in the pump improve power efficiency, help to regulate peak flow rates, and provide fluid storage. Owing to the large time constants associated with expelling fluid from the pump chamber through microfluidic channels with large resistance, valves would need to be held open for several seconds in some circumstances in order for the pump chamber to have time to fully drain/fill. However, capacitors between the pump chamber and the high-resistance microfluidic channels enable fast transfer of fluid into and out of the pump chamber followed by passive fluid flow associated with the pressure equilibration of the capacitors. This minimizes the amount of time valves need to be held open (to on the order of tens of milliseconds) and therefore reduces power consumption. In addition, the capacitor at the outlet attenuates flow rate bursts generated by pump strokes, reducing large peak flow rates to safer levels.

The fluidic capacitors in the micropump (including the pump chamber) are cylindrical chambers whose ceilings are a thin (25.4 μm), flexible, polyimide membrane. The diameter is the critical design dimension in these chambers that determines capacitance.[33] The pump chamber has a diameter of 3.5 mm, the fluidic storage capacitor has a diameter of 14 mm, and all of the remaining capacitors (outlet and both reservoir capacitors) have diameters of 4 mm. The same membrane is deflected to block flow at each of the valves. The valve chambers have diameters of 3.1 mm. The serpentine channel that comprises the drug reservoir has a square cross section of width 762 μm and a length of 410 mm for a total volume of 238 μL. All of the other microchannels in the pump have a width of 400 μm and a height of 254 μm.

2.2 Materials and Reagents

Polyetherimide (PEI) sheets of various thicknesses including 0.254 mm, 1.5875 mm, and 3.175 mm were obtained from McMaster Carr (Robbinsville, NJ). Polyimide sheets (76-μm and 25-μm thick) were purchased from Fralock (Valencia, CA). We purchased 0.25-mm Viton sheets from AAA-Acme Rubber Company (Tempe, AZ). R/flex 1000 bonding films (12.7 μm thick) were obtained from Rogers Corporation (Chandler, AZ). Prototyping board used for PCB fabrication (double-sided, copper-clad and 1.5875 mm thick) was purchased from Digi-Key (Thief River Falls, MN).

Stainless-steel type 316 hypodermic tubing of sizes 22-Ga (0.711 mm OD/0.406 mm ID) and 28-Ga (0.356 mm OD/0.178 mm ID) was purchased from Vita Needle (Needham, MA). Two sizes of polyether ether ketone (PEEK) tubing (360 μm OD/150 μm ID and 360 μm OD/100 μm ID) were purchased from IDEX Health & Science (Oak Harbor, WA). Tygon tubing (0.76 mm OD/0.25 mm ID) for use in cannula fabrication was purchased from Amazon (Seattle, WA). 2.08 mm OD/0.25 mm ID and 1.524 mm OD/0.508 mm ID Tygon tubing was purchased from Cole Parmer (Vernon Hills, IL). Polytetrafluoroethylene (PTFE) tubing for use in device characterization (3.17 mm OD/1.57 mm ID)

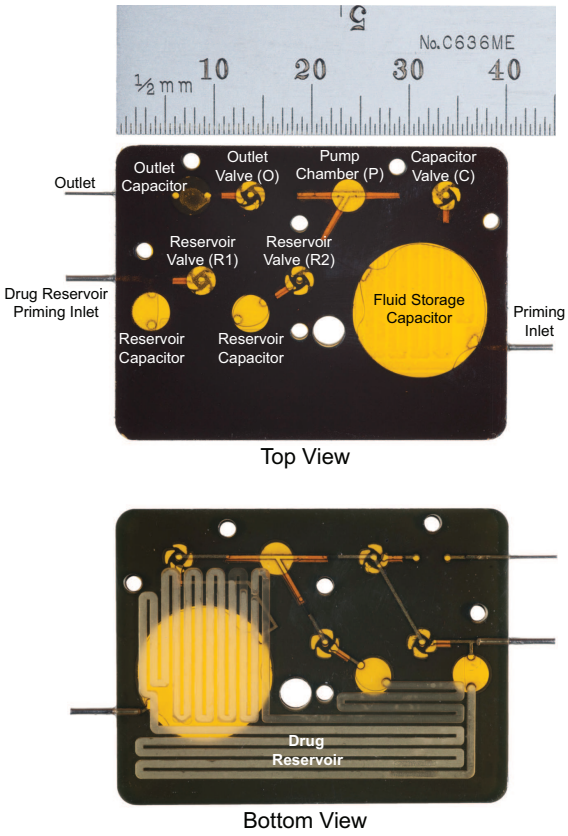

Fig. 3 Top and bottom back lit photographs of the microfluidics portion of our micropump. Several polymer layers were laminated together to form the 3-D microfluidic structures. The actuator locations are identified by O, P, C, R1, and R2.

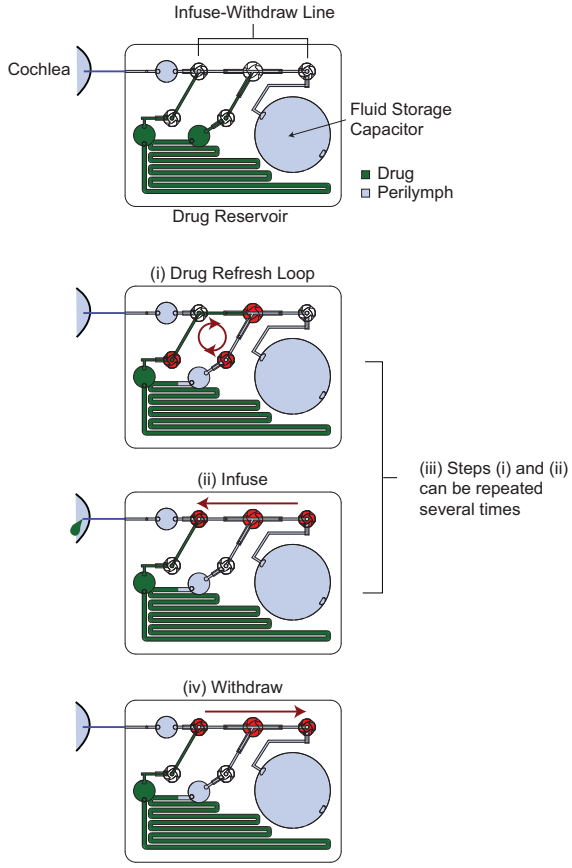

Fig. 4 Scheme showing the process flow for one drug delivery cycle, including drug refresh, infuse, and withdraw steps. All of the valves are normally closed, and open when power is supplied. Actuators/valves that are active and supplied power at some point during a particular step are highlighted in red. A simplified version of the drug reservoir is shown for clarity.

was purchased from Waters (Milford, MA). PTFE tubing for use in cannula fabrication (201 μm OD/101 μm ID) was purchased from Zeus Inc. (Branchburg, NJ). The tubing was etched by the manufacturer to facilitate binding to adhesives. We fabricated a cannula for insertion into the cochleostomy from the PEEK, Tygon, and PTFE tubing as described in our previous work.[26]

The glutamate receptor antagonist, 6,7-dinitroquinoxaline-2,3-dione (DNQX), was purchased from Fisher Scientific (Waltham, MA). All other chemicals and reagents were purchased from Sigma Aldrich (St. Louis, MO). Fluorescein solution was prepared by dissolving fluorescein in deionized water at a concentration of 0.1 mg/ml. Artificial perilymph (AP) solution was prepared by combining the following reagents, in mM: NaCl, 120; KCl, 3.5; $CaCl_2$, 1.5; glucose, 5.5; HEPES, 20. The AP was titrated with NaOH to adjust its pH to 7.5 (total Na^+ concentration of 130 mM).[27] DNQX solution comprised DNQX dissolved in AP at a concentration of 300 μM.

2.3 Pump Fabrication

We fabricated the microfluidics portion of our micropump by machining features into polymer sheets, and then laminating them together, as has been described in our previous work.[26,33] Features for each layer (Figure 5) were designed using SolidWorks software and converted for use with machining equipment using in-house written MATLAB scripts. Several different materials were used in building the microfluidic structure (Table 1) including: PEI for rigid structures, polyimide for flexible membranes, and Viton for compliance/fluidic sealing. Layers 1 and 9 were machined using a Quickcircuit 7000 XY router table (T-Tech, Norcross, GA), and layers 2–7 were cut with a LPKF ProtoLaser U3 UV Laser (LPKF Laser & Electronics, Garbsen, Germany). The cover (layer 10) was manufactured by the machine shop at Draper.

The fluidic layers 1–6 were laminated together at high temperature and pressure (175°C, ramped at 5°C/min, and then held for 1 hour; 2000 kPa effective pressure) using R/flex 1000 bond-

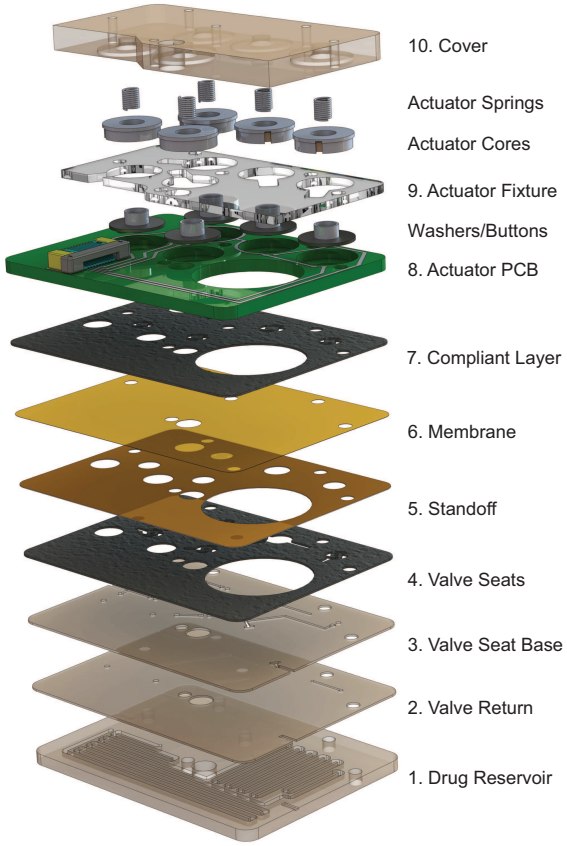

Fig. 5 Scheme showing an exploded view of the layers and structures that comprise our micropump. The layers numbered (1–6) were laminated together to form the microfluidics portion of the pump shown in Figure 3. The microfluidics and remaining layers were fastened together with bolts (Figure 1). Detailed descriptions of the materials are shown in Table 1.

ing films interspersed between the layers. Lamination was done in 3 stages. First layers 1–3 were laminated together. Next, the bottom side of layer 4 was treated with oxygen plasma (PX-250 Plasma Chamber, March Instruments, Concord, MA) for 1 min at a power of 150 mW and a pressure of 280 mTorr in an oxygen-argon atmosphere with 30% O_2. Layer 4 was then laminated to layers 1–3. During plasma cleaning and lamination, the Viton layer was fixed in a custom-machined annular clamp in order to keep it flat. The top side of layer 4 (now laminated to the other layers) was also treated with oxygen plasma. Finally, layers 5 and 6 were laminated to the rest of the stack. During the final lamination, layer 6 (the 25-μm polyimide membrane) was held under tension at 1.5% strain. After lamination, 0.75-cm lengths of 22-gauge stainless-steel tubing were inserted into the drug reservoir priming inlet and priming inlet. A 0.75-cm length of 28-gauge stainless-steel tubing was inserted into the outlet. Epoxy was then applied to all of the stainless steel tubing and allowed to cure.

Table 1 List of the layers that comprise our micropump, including materials and thicknesses. The layers are numbered starting from the bottom of the stack, and the numbers correspond to those shown in Figure 5.

#	Description	Material	Thickness	Machining
1	Drug Reservoir	PEI	1.5875 mm	Conventional
2	Valve Return	PEI	254 μm	UV Laser
3	Valve Seat Base	PEI	254 μm	UV Laser
4	Valve Seats	Viton	254 μm	UV Laser
5	Standoff	Polyimide	76 μm	UV Laser
6	Membrane	Polyimide	25 μm	UV Laser
7	Compliant Layer	Viton	254 μm	UV Laser
8	Actuator PCB	Proto Board	1.5875 mm	Conventional
9	Actuator Fixture	Acrylic	1.016 mm	Conventional
10	Cover	PEI	3.175 mm	Conventional

The actuator printed circuit board (PCB), layer 8, was routed from copper-clad prototyping board using the Quickcircuit 7000 router. A 10-pin, 0.5-mm pitch zero-insertion-force connector (Samtec ZF5S, Samtec, New Albany, IN) was soldered onto the PCB and used to connect the PCB to a custom-made controller via a Samtech FJH 0.5 mm flat flexible cable. An in-house written Lab View script was used to run the controller via a NI USB-6501 Digital I/O device (National Instruments, Austin, TX). For the experiments described here, the controller was large (approximately 10 cm x 20 cm x 5 cm) and powered from a wall outlet, but the control circuitry can be miniaturized and powered by battery. Annular electromagnets were custom-machined in house as described previously.[26] Leads from the magnets were soldered to the actuator PCB.

2.4 Pump Operation

In the fully assembled pump, the electromagnets are held in place by the acrylic actuator fixture (layer 9) and surface-mounted to the membrane side of the laminated microfluidic structure with a compliant, Viton layer in between (layer 7). The full structure is secured by bolts inserted from the bottom of the laminated fluidic stack and threaded into the cover (layer 10) situated at the top of the pump. When the electromagnets are unpowered, springs keep the actuator heads (polycarbonate buttons inserted into the centers of washers) pressed against the fluidic layers, deflecting the polyimide membrane onto the Viton valve seats resulting in a fluidic seal (closed valves). A valve is opened by applying a 12-V spike voltage to the corresponding electromagnet for 2 ms, and is then held open for a chosen amount of time (nominally 20 ms) by a 2-V hold voltage.

Cycling the actuator located above the pump chamber results in fluid displacement, and cycling any two valves in a particular sequence along with the pump chamber results in net flow through the device. In general, one valve acts as the intake valve, and another valve acts as the expulsion valve. At the beginning of a pump stroke, the intake valve opens, and then the pump actuator

Table 2 Summary of different pump stroke types. For each type, the actuator firing sequence is shown from left to right. Actuators that are in the powered state are shaded in green. Valves are normally closed, and are opened when power is supplied to their associated actuators (i.e., valves shaded in green below are open). The times listed in each sequence indicate the amount of time the indicated actuators are held in the powered state (at 2V). When an actuator is switched from unpowered to powered, a 2-ms, 12-V spike voltage precedes the hold. The flow path is indicated with red arrows along with the stroke type. A simplified representation of the drug reservoir is shown for clarity.

Stroke Type	Actuator Sequence					
	Intake Valve Opens	Intake	Intake Vale Closes	Expulsion Valve Opens	Expulsion	Wait for Equilibration
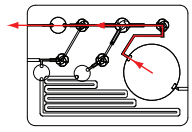 Infuse	C (6 ms)	C-P (20 ms)	P (6 ms)	P-O (6 ms)	O (20 ms)	Idle (5 s)
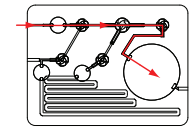 Withdraw	O (6 ms)	O-P (20 ms)	P (6 ms)	P-C (6 ms)	C (20 ms)	Idle (5 s)
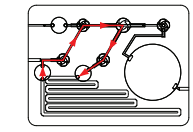 Drug Refresh	R1 (6 ms)	R1-P (20 ms)	P (6 ms)	P-R2 (6 ms)	R2 (20 ms)	Idle (5 s)

is powered resulting in fluid being drawn into the pump chamber from an adjacent fluidic capacitor. Next, the intake valve closes. Then the expulsion valve opens, followed by deactivation of the pump actuator, resulting in fluid being pushed out of the pump chamber into a different fluidic capacitor. Finally, the expulsion valve closes. Depending on which valves are chosen as the intake and expulsion valves, the pump can produce three different types of pump strokes (Table 2): infuse (fluid is pumped out of the pump), withdraw (fluid is pumped from an external source into the pump), and drug refresh (fluid is pumped in a loop within the pump, resulting in the transfer of drug out of the reservoir and into the main infuse-withdraw line). A full pump stroke cycle for any of these stroke types dissipates approximately 0.15–0.2 J.

2.5 Pump Performance Characterization

For the infuse and withdraw pump stroke schemes shown in Table 2, we characterized pump performance by measuring the volume transferred per pump stroke, the stroke volume. For these measurements, the pump was primed with deionized water, and the priming inlet of the pump was connected to a water reservoir via 0.508-mm ID Tygon tubing. The drug-reservoir priming inlet was blocked, and the outlet was connected to a piece of 1.57-mm ID PTFE tubing, with a fluidic resistor (consisting of a chosen length of 100-μm ID PEEK tubing) between the outlet and the PTFE tube. Short pieces of 0.25-mm ID Tygon tubing were used to make the connections between the outlet, PEEK tubing, and PTFE tubing. 40 pump (infuse or withdraw) strokes were actuated, resulting in water being pumped into or out of the PTFE tubing. The distance of travel of the air-water meniscus was measured and used to infer the total volume pumped. The total volume was then divided by 40 to get the stroke volume.

We measured instantaneous flow rates generated at the outlet of the pump by using a Sensirion SLI-0430 Liquid Flow Meter (Sensirion, Stäfa, Switzerland). For all instantaneous flow rate measurements, 9 cm of 100-μm ID PEEK tubing were attached to the outlet of the pump, and the flow sensor was attached to the PEEK, with pieces of 0.25-mm ID Tygon tubing used as connectors. Data was sampled from the flow sensor every 6 ms.

2.6 Verification of Electronically-Controlled Dosing

We characterized the pump's electronically-controlled dosing capabilities (i.e. the drug refresh pump stroke) by loading the drug reservoir in the pump with fluorescein solution and then measuring the fluorescence output from the pump. For these experiments, the priming inlet was connected to an external water reservoir via Tygon tubing. In order to prime the drug reservoir, we removed springs from actuators O, P, and R2. As a result, only the valves, R1 and C were closed. Fluorescein solution was then

pumped by hand using a syringe into the drug-reservoir priming inlet until it could be seen dripping from the outlet (at least 0.5 ml). The drug-reservoir priming inlet was then blocked by replacing the connected Tygon tubing with a short piece of tubing that had been blocked on one end with epoxy. The pump was then reassembled with springs only in the R1 and R2 positions. Water was then flushed by hand from the priming inlet to the outlet until all of the fluorescein solution was removed from the infuse-withdraw line (the flow path shown for the infuse stroke in Table 2). A 9-cm length of 100-μm ID PEEK tubing was then connected to the outlet via 0.25-mm ID Tygon tubing and also flushed with water. The pump was then reassembled with springs in all of the actuator positions. The priming inlet was then connected to an external water reservoir.

Sixty wells of a standard, opaque 96-well plate (Costar 96-well black solid plate, Corning Life Sciences, Tewksbury, MA) were each loaded with 100 μL of deionized water. 10-μL aliquots dispensed by the pump (comprising 20 infuse strokes each) were collected in successive wells. For the 1st aliquot and every 6th aliquot thereafter (i.e., 1, 7, 13, etc.), drug-refresh pump strokes were actuated prior to the infuse pump strokes. Three different dosing cases were tested where the infused volume and hence the number of infuse strokes was kept constant, but the number of drug refresh strokes was varied; one drug-refresh stroke per infuse stroke (20 refresh strokes total), one drug-refresh stroke per two infuse strokes (10 refresh strokes total), and one drug-refresh stroke per three infuse strokes (7 refresh strokes total and 21 infuse strokes total for this case only). Fluorescence in the wells was then measured using a plate reader (SpectraMax M2, Molecular Devices, Sunnyvale, CA) with excitation at 490 nm and emission at 514 nm, and the raw fluorescence data was converted to concentration through the use of standards.

2.7 Surgical Procedures and Hearing Tests

All surgical procedures used in this study were approved by the Massachusetts Eye and Ear Infirmary Institutional Animal Care and Use Committee. Four male, albino, guinea pigs, each weighing approximately 350 g, were obtained from Charles River Laboratories, Inc. (Hartley strain; Wilmington, MA). The guinea pigs were anesthetized using a combination of pentobarbital sodium (Nembutal; 25 mg/kg, injected intraperitoneally), fentanyl (0.2 mg/kg, intramuscularly), and haloperidol (10 mg/kg, intramuscularly). Lidocaine with epinephrine was given subcutaneously at the incision site as a topical anesthetic. Half doses of each drug were given at first. A 0.04 mg/kg dose of atropine was given subcutaneously at that time as well to reduce secretion in the airway. Additional half doses of each anesthetic were administered approximately hourly in order to maintain the appropriate depth of anesthesia during drug delivery and hearing tests.

Using a dorsal approach, a small hole (~5 mm in diameter) was made in the bulla, then a cochleostomy was created approximately 0.5 mm distal to the round window membrane. The cannula coming from the micropump was inserted into the cochleostomy, threaded into the cochlea 3 mm apically, and glued to the bulla with a common cyanoacrylate glue. For compound action potential measruements, a perfluoroalkoxy-alkane-insulated silver wire electrode (203 μm uncoated diamter, A-M systems, Carlsborg, WA) was inserted near the round window niche and glued to the bulla.

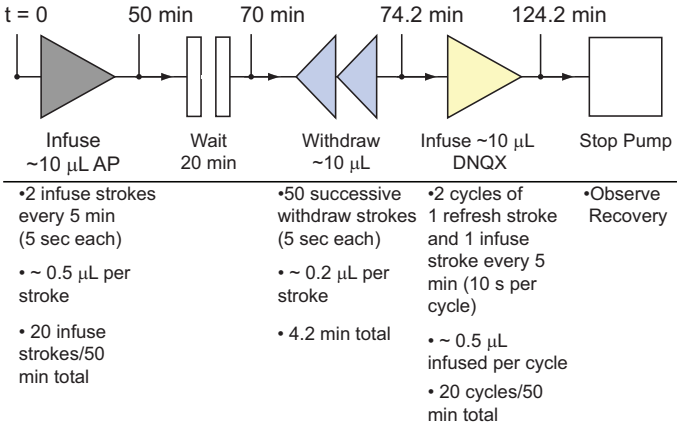

Fig. 6 Chart describing the flow of drug delivery experiments in guinea pigs. The approximate timing of each experimental phase is listed. In a real experiment, there were additional delays for set up time.

Procedures for measurement of distortion product otoacoustic emissions (DPOAEs) and compound action potentials (CAPs) have been described in our previous work.[26] DPOAEs were measured before and after the cochleostomy procedure (at the characteristic frequencies: 32, 24, 16, 12, 8, 5.6, 4, and 2.78 kHz) in order to monitor any damage that may have occurred as a result of the surgery.

2.8 Acute Drug Delivery in Guinea Pigs

For acute drug delivery experiments in guinea pigs, we first primed the drug reservoir in the pump with DNQX solution using the same procedure used for fluorescein described in Section 2.6. Next, the drug reservoir priming inlet was blocked, 9-cm of 100-μm ID PEEK tubing and the cannula were attached to the outlet of the pump, and the rest of the pump along with the outlet tubing was primed with AP. Once the main infuse-withdraw line and outlet tubing had been sufficiently flushed with AP so as to remove the DNQX solution, the priming inlet was blocked.

The cannula was then inserted into a cochleostomy made in the region of the cochlea between 24 and 32 kHz and threaded apically 3 mm, terminating in the 12–16 kHz region. We then performed DPOAE and CAP hearing tests to serve as baseline measurements prior to the start of AP/drug infusion. The pump was

then activated, initiating delivery of fluids into the cochlea in the sequence described in Figure 6. Approximately 1 μL of AP were infused (by actuating 2 infuse strokes) every 5 min until a total of approximately 10 μL of AP were delivered to the cochlea over 50 minutes (20 infuse strokes in total). After a 20 min wait time, approximately 10 μL of fluid were withdrawn from the cochlea by actuating 50 withdraw strokes (more withdraw strokes are necessary compared to infuse strokes because the withdraw stroke volume was smaller than the infuse stroke volume, as discussed in sections 3.1 and 4.1). Finally, we initiated DNQX delivery (approximately 1μL every 5 min) by actuating 2 cycles of 1 drug refresh pump stroke and 1 infuse pump stroke every five minutes, until a total of 20 cycles had been actuated (again, approximately 10μL of fluid delivered over 50 min).

During infusion, we repeated measurements of CAPs generated in response to tone-pips at 32, 24, 16, 12, and 8 kHz as quickly as possible (approximately every 20 minutes). Based on our previous work,[26] we did not expect the DNQX to reach more apical frequencies in this time frame, so we omitted those measurements in favor of greater time resolution. We also measured DPOAEs during infusion (including at the more apical frequencies of 5.6, 4, and 2.78 kHz), but only approximately hourly (DPOAEs were not expected to change, so high temporal resolution was not necessary for those measurements). Before each DPOAE measurement, we checked the middle ear for perilymph that may have leaked from the cochleostomy, and removed any fluid that was present by aspiration.

After the end of DNQX infusion, we continued to monitor hearing for nearly 3 hours in order to observe recovery. During recovery, we measured CAPs in response to the apical frequencies as well, and continued to monitor DPOAEs hourly.

2.9 Data Analysis

We calculated CAP amplitudes by subtracting the minima of the waveforms from the maxima. Peaks that were artifacts of filters in the acoustic system were ignored in this analysis. The CAP threshold was taken to be the minimum tone-pip sound pressure level (SPL, a measure of sound exposure) that generated a CAP response with an amplitude of at least 0.5 μV. If a tone-pip with SPL of 100 dB did not generate a CAP amplitude equal to or greater than 0.5 μV, the threshold shift was set to 120 dB. CAP thresholds and amplitudes were grouped into 20-min bins so that they could be averaged across biological replicates.

DPOAEs are sounds generated in the cochlea when it is stimulated by two pure tone frequencies, f_1 and f_2, when the ratio of f_2 to f_1 is between 1.1 and 1.3. They serve as an indicator for hair cell function. For DPOAEs, we measured the magnitude of the $2f_1 - f_2$ response (typically the most prominent distortion product), where f_2 was the characteristic frequency, and $f2/f1$ was 1.2. The SPL of f_1 was 10 dB greater than that of f_2. The noise floor at a frequency, f, was calculated from the DPOAE magnitude spectrum as the average of the magnitudes at 2 frequency samples above f, and 2 frequency samples below f. The threshold was the minimum SPL required to generate a $2f_1 - f_2$ magnitude that was greater than the noise floor at $2f_1 - f_2$. DPOAEs were measured at approximately the same time in each experiment relative to the start of drug delivery, so they were averaged across biological replicates directly.

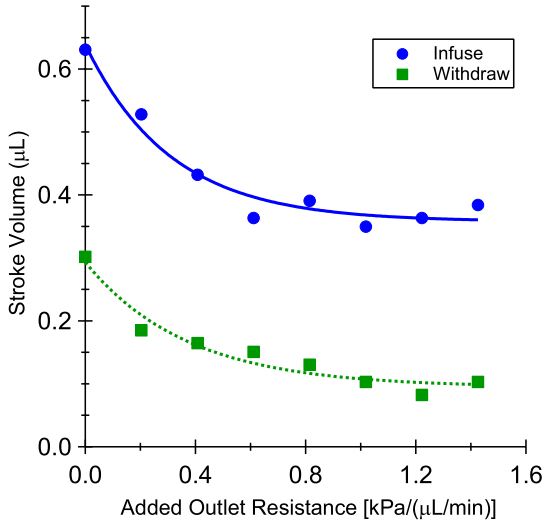

Fig. 7 Volume delivered (or withdrawn) per stroke of the micropump as a function of hydrodynamic resistance added to the outlet. A 9-cm length of 100-μm ID PEEK, as was used in our fluorescence and animal experiments, corresponds to a resistance of 0.61 kPa/(μL/min). Exponential fits are shown to help guide the eye. Hydrodynamic resistances shown here and throughout this work were calculated using the standard relation derived from Hagen-Poiseuille flow.

3 Results

3.1 Infuse/Withdraw Performance Characterization

We characterized the micropump's ability to generate flow in both the forward (infuse) and reverse (withdraw) directions against different loads by measuring the stroke volume as a function of outlet resistance (Figure 7) for the standard pump stroke paradigms shown in Table 2. We used different lengths of 100-μm ID PEEK tubing attached to the outlet to add resistance. With no load, the infuse pump stroke volume was 0.63 μL, and it decreased to approximately 0.38 μL with increasing outlet resistance. The withdraw stroke followed the same general trend, but the stroke volume was less than half of the infuse stroke volume for all loads. Based on these data, we chose to operate our pump with 9 cm of 100-μm ID PEEK tubing attached to the outlet (corresponding to a hydrodynamic resistance of 0.61 kPa/[μL/min]) for our drug infusion experiments. Pump performance and added outlet dead volume (0.71 μL) were acceptable with this configu-

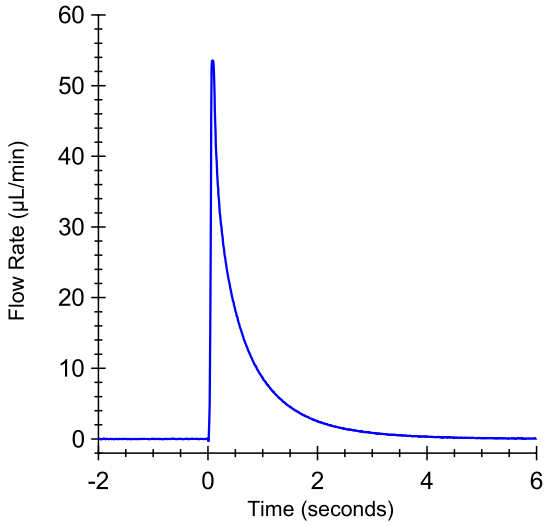

(a)

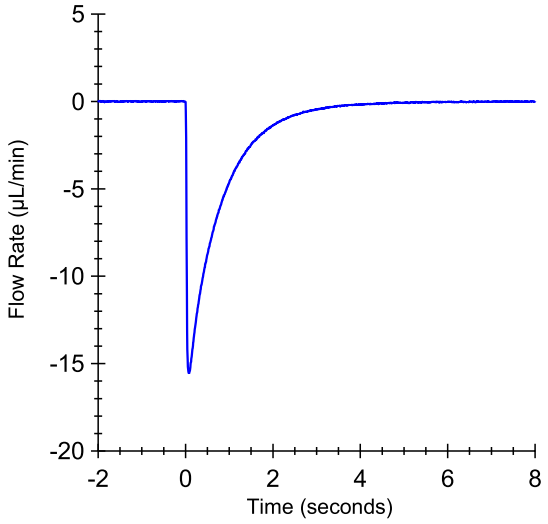

(b)

Fig. 8 Flow rate generated by the pump as a function of time after (a) a single infuse pump stroke and (b) a single withdraw stroke. A 9-cm length of 100-μm ID PEEK was attached to the outlet. The volume of the infuse stroke was 0.47 μL, and the volume of the withdraw stroke was 0.22 μL.

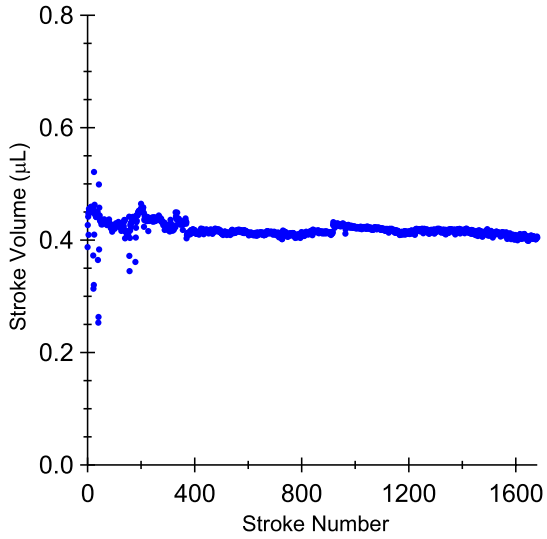

Fig. 9 Infuse stroke volume is consistent over more than 1600 strokes after some initial scatter (likely due to air settling in the system). For these data, the pump was set to repeatedly generate infuse strokes. A 9-cm length of 100-μm ID PEEK and the flow sensor were attached to the outlet. Stroke volumes were calculated by integrating the flow sensor data. The average stroke volume was 0.42 $\pm$ 0.02 μL.

ration, and the outlet tubing was still long enough to travel from the pump to a cochleostomy in a guinea pig.

With the pump configured as described above, we measured instantaneous flow rates generated at the outlet during infuse and withdraw pump strokes using the Sensirion Liquid Flow Meter. The flow sensor was oriented such that positive flow rates indicate fluid leaving the pump, and negative flow rates indicate fluid entering the pump. At the beginning of of a typical infuse pump stroke (Figure 8a), there is small negative flow (-0.35 μL/min) resulting from the expulsion valve opening, followed by a much larger spike in positive flow (54 μL/min) corresponding to expulsion. The flow rate then decays approximately exponentially to zero over a period of approximately 5 seconds as the outlet capacitor drains. For a typical withdraw pump stroke (Figure 8b), the expulsion valve is isolated from the flow sensor, so the small response to the valve opening is not observed, and there is only a large flow rate spike (-16 μL/min) followed by decay. To test the infuse stroke consistency, we configured the pump with the flow sensor as described above and actuated 1680 pump strokes (Figure 9). We measured a mean stroke volume of 0.42 μL with a standard deviation of less than 4%.

We also examined how variation of the the intake time during a pump stroke affects stroke volume (i.e. the time the intake and pump actuators are powered; nominally 20 ms as shown in Table 2). During these experiments, the expulsion valve hold time was set to 200 ms. Increasing the intake time led to an increase in stroke volume (Figure 10) for both the infuse and withdraw pump

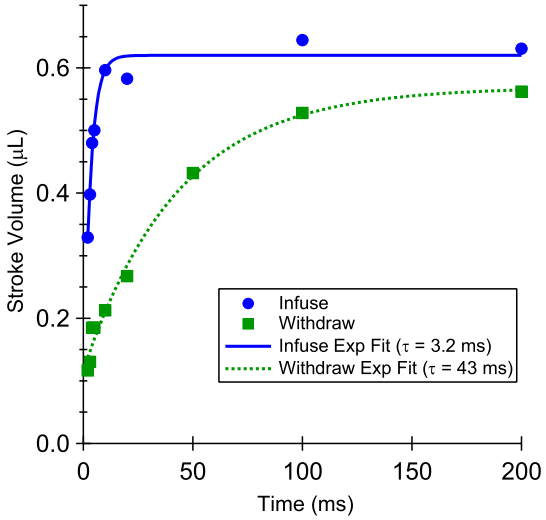

(a)

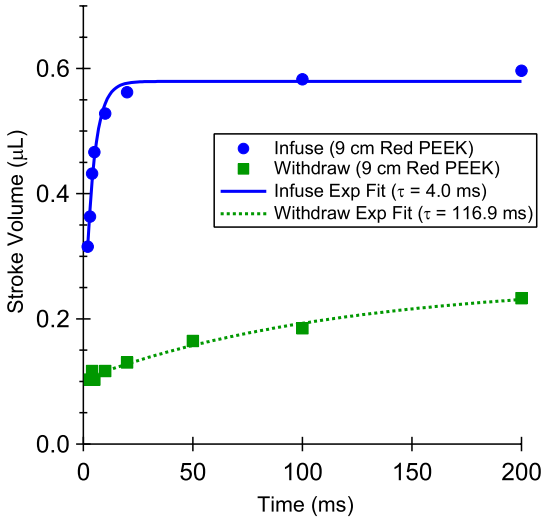

(b)

Fig. 10 Volume delivered (or withdrawn) per pump stroke as a function of intake time (the amount of time the intake valve and pump actuators are held in the powered state). In (a), no resistive tubing was added to the outlet, so the outlet resistance was low—approximately 5.4 Pa/(μL/min)—while in (b), 9 cm of 100-μm ID PEEK tubing were attached to the outlet, bringing the total outlet resistance to 0.62 kPa/(μL/min). For all of these data, the expulsion valve hold time was set to 200 ms, and the inlet resistance was 0.9 Pa/(μL/min).

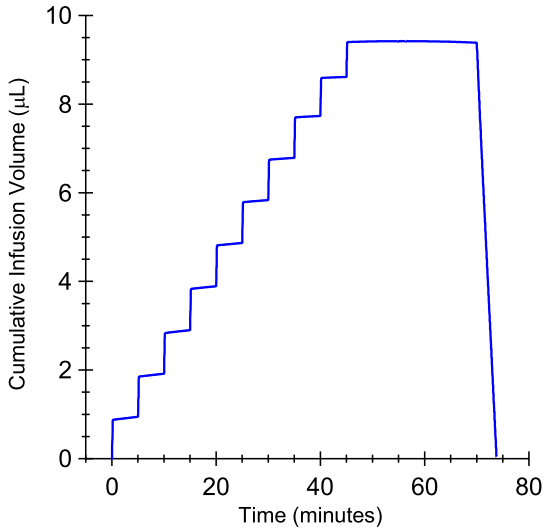

Fig. 11 Bench-top measurement of the fluid volume output of the pump as a function of time for the same reciprocation profile used in our animal experiments. We could not use a flow sensor to measure volume output during animal experiments, because attaching a flow sensor inline at the pump outlet adds unacceptable dead volume. For this profile, two infuse strokes were pumped every 5 min., 10 times (20 total infuse pump strokes with a total volume of 9.4 μL). After a 20 min wait, 45 withdraw strokes were pumped bringing the total infusion volume back to nearly zero.

strokes. When no additional hydrodynamic resistance was added to the outlet of the pump, the variation of stroke volume with intake time followed an exponential form, with a time constant of 3.2 ms for the infuse pump stroke, and a much longer time constant of 43 ms for the withdraw pump stroke. When 9 cm of 100-μm ID PEEK tubing were added to the outlet, the relationship between intake time and stroke volume remained essentially the same for the infuse pump stroke. For the withdraw pump stroke, however, the time constant nearly tripled to 117 ms.

During drug delivery, fluid is pumped out from the large fluid-storage capacitor, and then withdrawn back into the capacitor at a later time. To test this reciprocating flow, we configured the pump with 9 cm of 100-μm ID PEEK tubing and the flow sensor attached to the outlet as described above, and both priming inlets were blocked. The outlet tubing of the flow sensor was inserted into a water reservoir. 2 infuse strokes were then actuated every 5 minutes, 10 times (a total of 20 infuse strokes). After a 20-min wait time, 45 withdraw strokes were actuated. The flow rate, measured as a function of time during this entire procedure, was integrated to yield the cumulative infusion volume as a function of time (Figure 11). The cumulative infusion volume increased by 0.94 μL during each of the 2-stroke infusion steps, and then decreased back to zero during the 45 withdraw strokes.

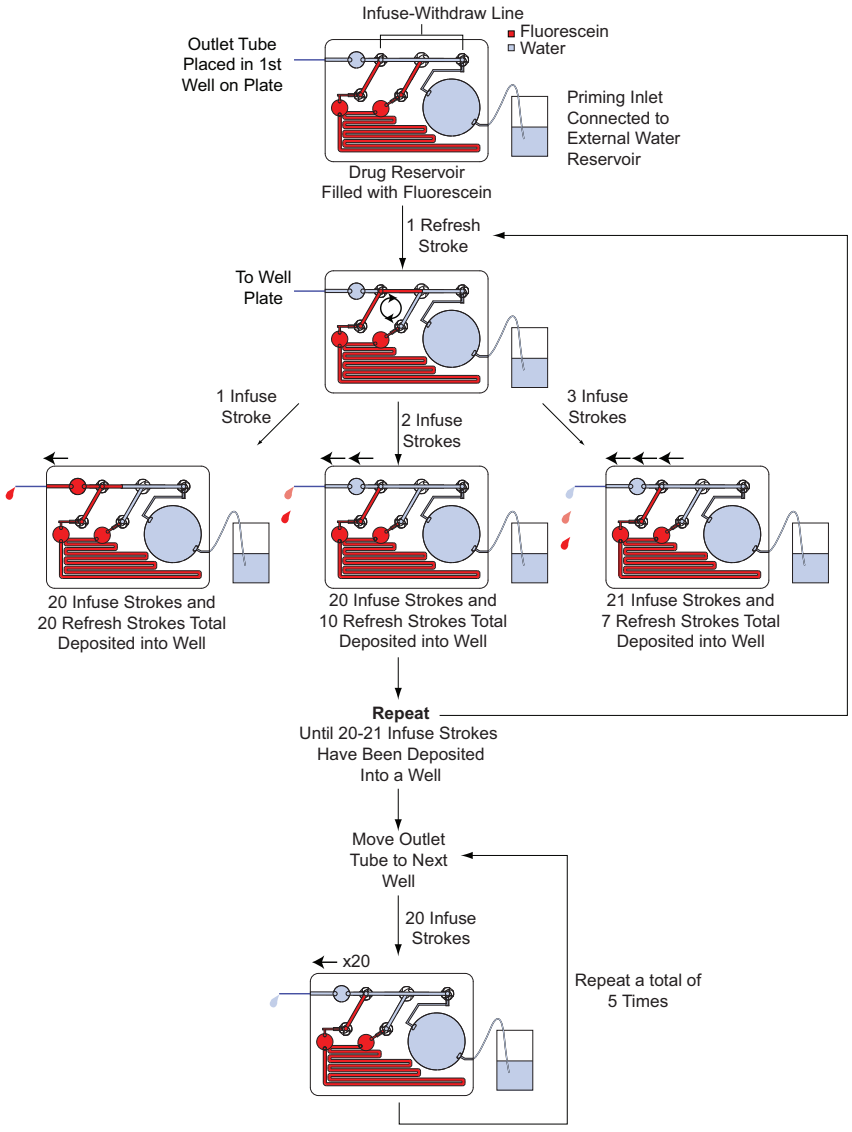

(a)

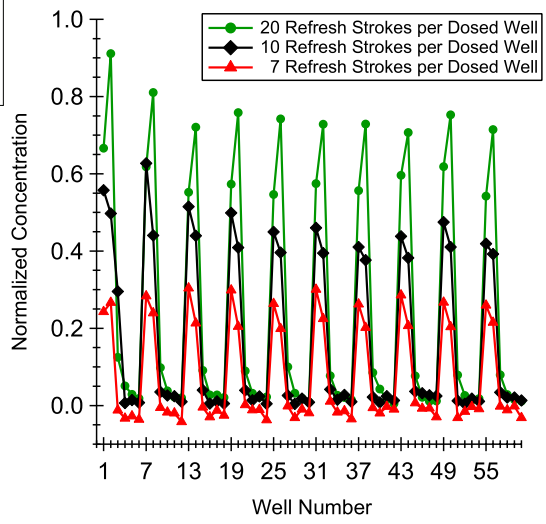

(b)

Fig. 12 Drug dosing is electronically initiated on demand. The effective concentration of drug delivered can be lowered by reducing the number of refresh strokes relative to the number of infuse strokes. (a) Scheme showing the process flow for fluorescence experiments that demonstrate 3 different dosing schemes. The drug reservoir in the pump was primed with fluorescein solution, while the rest of the pump was primed with deionized water. A higher ratio of infuse to refresh strokes leads to increased dilution of the dose. Note that some dilution occurs in all dosing schemes due to the dead volume ($\sim 4\ \mu$L) that must be cleared at the start of the dose. The entire process was repeated 10 times in subsequent wells on the microplate to generate the data shown in (b), resulting in a total of 60 aliquots collected sequentially in individual wells. (b) 10-μL aliquots (20 infuse strokes each) dispensed by the pump were collected in successive wells in a 96-well plate. For the first aliquot and every 6th aliquot thereafter (i.e. first, seventh, thirteenth, etc.), drug refresh strokes were actuated prior to the infuse strokes according to one of the schemes shown in (a). The fluorescence data was normalized to the initial fluorescein concentration (0.1 mg/ml).

3.2 Drug Refresh Loop and Electronically-Controlled Dosing

Because we did not have a precise method for monitoring flow rates/stroke volumes within the pump during a drug refresh pump stroke, we used fluorescein as a test drug to measure drug output from the pump with electronically-controlled dosing. We wanted to ensure that (1) drug was successfully transferred from the drug reservoir to the main infuse/withdraw line and ultimately out of the pump, (2) drug doses could be delivered on demand, (3) no drug was infused when drug refresh strokes were not actuated, and (4) dosing was reasonably repeatable/controllable. Based on these criteria, we evaluated the pump by collecting ∼10-μL aliquots (comprising 20–21 infuse pump strokes each) dispensed by the pump into successive microplate wells. We actively dosed only every 6^{th} aliquot with fluorescein, starting with the 1^{st} well (Figure 12a).

We tested three different dosing schemes, where the total number of infused strokes was held constant (20–21 strokes) and we varied the number of refresh strokes: 1 drug refresh stroke for every infuse stroke (20 refresh strokes total), 1 refresh stroke for every 2 infuse strokes (10 refresh strokes total), and 1 refresh stroke for every 3 infuse strokes (7 refresh strokes total). For any aliquot that was dosed with fluorescein, one of these schemes was repeated until a total of 20 (21 for the 7-refresh-stroke scheme) infuse pump strokes had been actuated. For all dose schemes, the actively dosed wells were fluorescent, indicating that fluorescein was successfully delivered to those wells (Figure 12b). The 20-refresh-stroke scheme produced the largest average dose, 0.58 $\pm$ 0.04 of the original fluorescein concentration (n = 10). The 10-refresh-stroke and 7-refresh-stroke schemes produced average doses of 0.48 $\pm$ 0.07 and 0.28 $\pm$ 0.02, respectively. For all schemes, the wells immediately following the actively dosed wells were also fluorescent, with normalized concentrations of 0.76 $\pm$ 0.06, 0.41 $\pm$ 0.04, and 0.22 $\pm$ 0.02 for the 20-refresh-stroke, 10-refresh-stroke, and 7-refresh-stroke schemes, respectively. For the 20-refresh-stroke scheme, these wells had a higher average concentration of fluorescein than the dosed wells, which likley resulted from the refresh stroke volume being significantly larger than the infuse stroke volume (see discussion). In subsequent wells following a dose, the fluorescein concentration quickly dropped to nearly zero.

3.3 Acute Intracochlear Drug Delivery in Guinea Pigs

We evaluated the safety and efficacy of using our micropump for acute intracochlear drug delivery. We started with reciprocating delivery of AP so that we could electronically switch to delivery of a test drug at a later time and demonstrate on-demand dosing. We used DNQX as our test drug, and monitored changes to hearing as a function of time and sound frequency in order to evaluate the efficacy of delivery. DNQX, a glutamate receptor antagonist that suppresses CAPs without affecting the DPOAEs,[34–36] has been used as a physiological indicator because frequency-dependent changes in CAP amplitudes and thresholds in response to DNQX delivery over time can be used to infer the distribution of drug in the cochlea.[18,24,26,27]

As expected, DPOAE threshold shifts were minimal during reciprocating AP delivery, DNQX delivery, and the recovery period following delivery at all frequencies tested ranging from 2.78–32 kHz (Figure 13). During AP infusion and withdrawal, CAP threshold elevations were smaller than 15 dB at all frequencies measured. After the start of DNQX delivery, CAP thresholds became more elevated at all frequencies monitored (8–32 kHz), where thresholds were elevated by at least 33 dB at all frequencies. The largest observed elevation (75 dB) occurred at 16 kHz at the end of DNQX delivery. The maximum threshold elevation at 8 kHz (33 dB) occurred approximately 1 hour after the pump was shut off, whereas the maximum elevations at the other observed frequencies (basal to or near the cannula site) occurred at or just after the end of DNQX delivery. CAP thresholds returned to normal when the pump was shut off, 1.5–2 hours after the maximum threshold elevation was observed.

In a manner consistent with the CAP threshold elevations, CAP amplitudes began to decrease after the start of DNQX delivery at all observed frequencies (Figure 14). For frequencies near the estimated cannula site (12 and 16 kHz) and all frequencies basal to that site, the minimum in CAP amplitude was observed at the end of DNQX delivery. At 8 kHz, a location apical to the cochleostomy site, the minimum CAP amplitude was observed approximately 1 hour after the pump was shut off. The largest reduction in CAP amplitude (a factor of 40) was at 16 kHz. There was less CAP amplitude suppression farther away from the infusion site, as amplitudes at 32 and 8 kHz were only reduced by a factor of 5–7. There was also some reduction in CAP amplitudes during reciprocating delivery of AP, which is most likely due to a small amount of DNQX that was left in the infuse/withdraw as an artifact of the pump priming procedure. During AP delivery, the largest decrease in CAP amplitude, also seen at 16 kHz, was a factor of 2.7 (as compared to the 40-fold reduction during the drug-delivery period). Following AP infusion, the 20-min wait time where the pump was off, and withdrawal of approximately 10 μL of fluid from the cochlea, CAP amplitudes recovered (increased) slightly at 32, 24, 16, and 12 kHz, while the amplitude decreased slightly at 8 kHz. The frequency-dependent reductions in CAP amplitudes (more clearly visualized in Figure 15) and recovery following withdrawal are consistent with delivery of a low concentration ($<$ 100 μM) of DNQX[26] during the first reciprocating delivery phase. As was the case with the CAP thresholds, after the pump was shut off following DNQX delivery, there was recovery (an increase in CAP amplitude) at all frequencies, and amplitudes returned to near-baseline levels approximately 1.5–2 hours after the minimum CAP amplitudes were observed. CAP

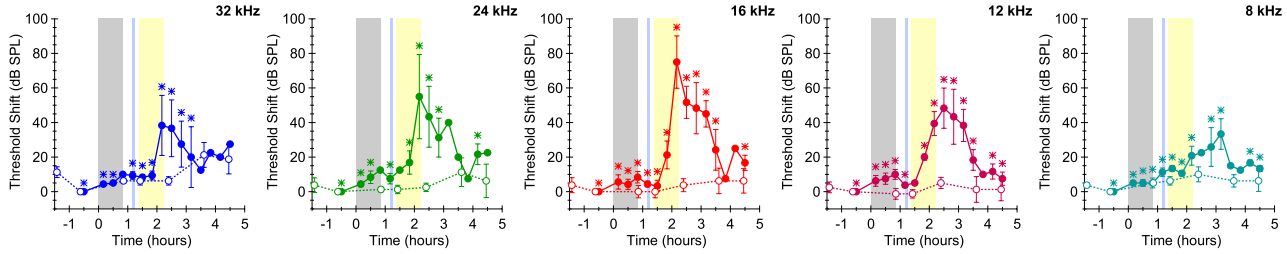

Fig. 13 CAP (solid lines, closed circles) and DPOAE (dashed lines, open circles) threshold shifts as a function of time during infusion of AP into, withdrawal of fluid from, and infusion of DNQX into a guinea pig cochlea. AP infusion began at t = 0, and shifts were calculated with respect to measurements taken just before t = 0. The gray shaded areas (t = 0 to t = 0.83 hours) represent the times during which artificial perilymph was infused. The blue shaded areas (t = 1.17 to t = 1.24 hours) represent the times during which fluid was withdrawn from the cochlea. The yellow shaded areas (t = 1.38 hours to t = 2.22 hours) represent the times during which a drug-refresh pump stroke was run prior to each infuse pump stroke, resulting in DNQX infusion into the cochlea. For non-shaded areas, the pump was idle. The asterisks for the CAP thresholds indicate data points that are the mean of either 3 or 4 biological replicates, and the error bars on those points represent the standard error of the mean. All other CAP threshold data points had fewer than 3 replicates. All DPOAE thresholds shown are the mean of 4 biological replicates, with error bars that represent standard error. In cases where there was no CAP response, CAP threshold shifts were set to 120 dB.

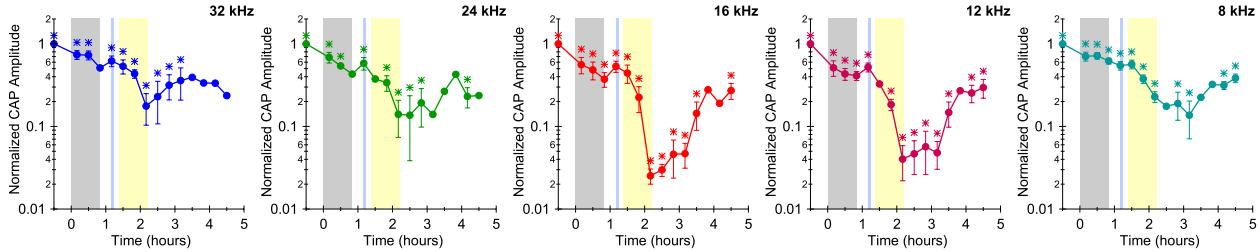

Fig. 14 CAP amplitude as a function of time in response to 60-dB tone-pip stimuli during infusion of AP into, withdrawal of fluid from, and infusion of DNQX into a guinea pig cochlea. See Figure 13 for notation.

amplitude suppression was not observed at any time during or after delivery for frequencies below 8 kHz (monitored only after the pump was shut off).

Distribution of drug through the cochlea over time was visualized through image plots of CAP amplitude and threshold shift (Figure 15). The effects of DNQX were first observed near the estimated cannula site at 12 and 16 kHz, and also quickly at frequencies basal to the cannula site. The DNQX began to spread toward the apex later. After the pump was shut off, recovery was observed at the most basal frequencies first, and at more apical frequencies later.

4 Discussion

4.1 Pump Performance

As shown in Figure 7, the pump maintained its ability to generate net flow in both the infuse and withdraw directions as the added outlet resistance was increased from 0 to 1.4 kPa/(μL/min). The hydrostatic pressure in the perilymph of typical guinea pigs ranges from 0.1–0.4 kPa,[37–41] so the pump can maintain fluid displacement against typical physiological pressures encountered at the flow rates described in this study with a safety margin for any clogs that may develop in the system. Furthermore, the pump delivers repeatable stroke volumes over more than 1000 pump strokes (Figure 9). Most of the scatter in the stroke volumes shown in Figure 9 is early in the experiment, and is most likely due to air bubbles settling in the system. Interestingly, the pump is less than half as effective at pumping fluid in the withdraw direction as it is in the infuse direction. This is due to a combination of low outlet capacitance and high outlet resistance. During the intake phase of a withdraw stroke, the pump actuator is powered, and the button above the pump chamber is retracted. This results in passive restoration of the membrane above the pump chamber, and fluid being drawn in from the outlet capacitor. Because this process is passive, it is driven by equalization of pressure between the pump chamber and the outlet capacitor.

During this equilibration, fluid will flow from outside the pump into the outlet capacitor, and both the pump chamber and outlet capacitor would ultimately come to pressure equilibrium with the external fluid source, given enough time. However, because the outlet resistance is high, the time scale for flow of fluid from outside the pump to inside the pump is long as compared to the amount of time the outlet valve is held open. In other words, the pump draws nearly the entirety of the stroke volume from the outlet capacitor.

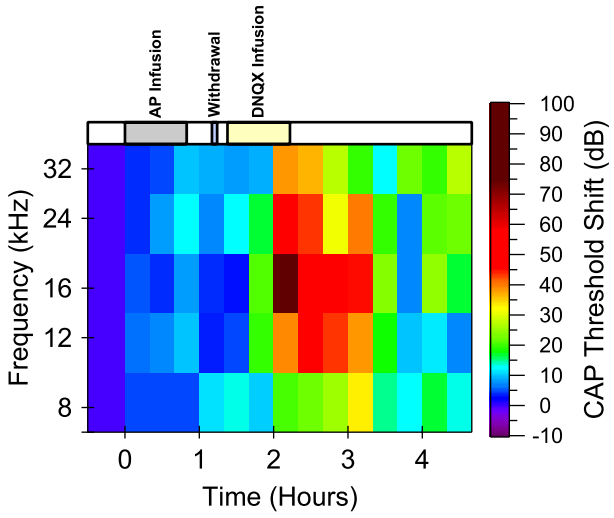

(a)

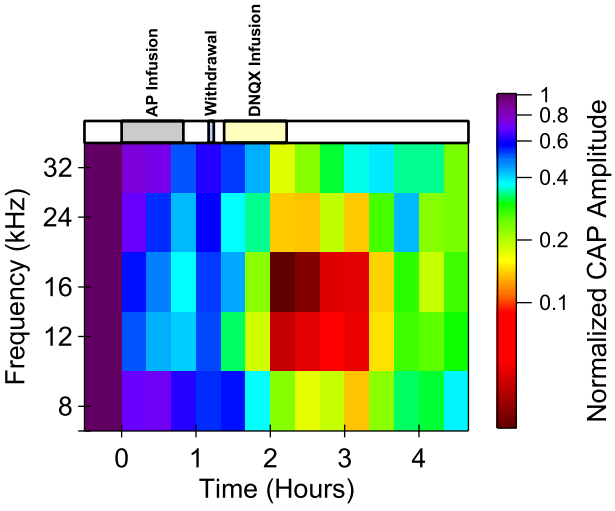

(b)

Fig. 15 Image plots of (a) CAP threshold shift and (b) normalized CAP amplitude as functions of time and frequency. Warmer colors represent greater hearing loss (larger threshold shifts, smaller CAP amplitudes). AP infusion began at t = 0, and regions of AP infusion, withdrawal, and DNQX infusion are indicated. For (b), the color bar is on a log scale, and the CAPs were generated in response to 60-dB tone-pip stimuli. Each pixel represents the mean of up to 4 biological replicates.

In our design, the outlet capacitor has a capacitance that is larger but comparable to that of the pump chamber (4 mm diameter vs. 3.5 mm diameter), so the equilibrium state is one where the pump chamber is not completely filled (the membrane does not fully restore to its flat, equilibrium position). For the infuse stroke on the other hand, the pump chamber draws fluid in from the much larger (14 mm diameter) fluid storage capacitor, so it is nearly completely filled during the intake phase, as removal of one stroke volume from the fluid storage capacitor minimally changes its pressure. The withdraw performance can be improved by increasing the diameter of the outlet capacitor in order to increase its capacitance,[33] but this would also increase its dead volume. We chose the diameter of the outlet capacitor as a compromise between withdraw stroke performance and dead volume.

We verified that the mechanism described above explains the reduced withdraw-stroke performance by examining the effect of intake-actuator hold time on stroke volume (Figure 10). We expected that increasing the amount of time that the intake and pump actuators were held in the powered state would allow for more fluid to be drawn into the pump chamber from outside the pump, resulting in increased stroke volume. By measuring the stroke volume as a function of intake time, we effectively measured the time constant for the pressure equilibration of the pump chamber with external fluid sources at atmospheric pressure.

For the infuse stroke, the RC time constant for this equilibration is defined by the inlet resistance, 0.9 Pa/(μL/min), and the equivalent capacitance of the fluid storage capacitor and the pump chamber in series. For the withdraw stroke, the time constant is defined by the outlet resistance—5.4 Pa/(μL/min) with no PEEK, and 620 Pa/(μL/min) with 9 cm of 100-μm ID PEEK—and the equivalent capacitance of the outlet capacitor and the pump chamber in series. Because the pump chamber capacitance, C_p, is smaller than either the outlet capacitance or the fluid storage capacitance, the equivalent capacitance for both the infuse and the withdraw falls between $C_p/2$ and C_p (For the infuse it is closer to C_p, and for the withdraw it is closer to $C_p/2$). The equivalent capacitance, therefore, differs between the infuse and withdraw by at most a factor of 2, so differences in the time constant between infuse and withdraw are dominated by differences in hydrodynamic resistance.

As expected, increasing the intake time increased the stroke volume following a saturating exponential form for both the infuse and withdraw strokes (Figure 10). The RC time constant for the withdraw intake was a factor of 13.4 larger than it was for the infuse intake, primarily due to the more resistive stainless steel tubing (28 Ga) at the outlet as compared to the inlet (22 Ga). The addition of PEEK tubing to the outlet did not affect the time constant for the infuse stroke much (it increased by a factor of 1.3), because that tubing was not involved in the intake phase

of the infuse stroke. The extra resistance from the PEEK tubing did, however, increase the time constant for the withdraw intake by a factor of 2.7.

4.2 Safe Flow Rates

In our work with our previous-generation infuse-only micropump,[26] we tried to limit peak flow rates to under 10 μL/min in order to prevent possible damage due to high flow rates. In that work, we increased the resistance at the outlet until flow rates were under 10 μL/min. We had used DPOAE data generated in previous studies,[18] in which a syringe pump was used for delivery, to estimate this maximum safe flow rate for this type of pulsed delivery (drug delivered in short bursts of flow at the maximum flow rate that last on the order of hundreds of milliseconds, at intervals on the order of minutes). Our current micropump design (with 9 cm of 100-μm ID PEEK tubing attached to the outlet) generates pulses of flow with peaks in the 45–55 μL/min range for infuse pump strokes, and in the 13–18 μL/min range for withdraw pump strokes (Figure 8).

For the current-generation micropump, we could not arbitrarily add resistance to the outlet of the pump in order to reduce peak flow rates, because we had to consider withdraw stroke performance and dead volume, parameters that are critical for reciprocating delivery. The addition of outlet resistance impacts the withdraw stroke more strongly than it impacts the infuse stroke, so we chose to add the maximum outlet resistance possible for which the withdraw stroke performance was still adequate. Increasing the outlet capacitance would alleviate the disparity between the infuse and withdraw strokes, but would also add unacceptable dead volume. Despite the fact that the peak flow rates generated by the current-generation device were a factor of 5 larger than our typical safety limit, we did not see evidence of mechanical damage during acute drug delivery (Figure 13, DPOAEs). In general, safety limits are not well-characterized, and our data from this study suggests that our original estimate of 10 μL/min is conservative for pulsed, acute delivery. However, these flow rates may still cause damage chronically.

4.3 Electronically Controlled Dosing

When we used fluorescein as a test drug, we saw a clear increase in fluorescence output from the pump when we initiated drug-refresh pump strokes (Figure 12). This demonstrates that our device is capable of on-demand, electronically-controlled dosing. For all of the dosing schemes we tested, the fluorescein dispensed by the pump was at a lower concentration than the the fluorescein solution we loaded into the pump's drug reservoir. There were approximately 4 μL of dead volume between the outlet valve and the end of the PEEK tubing that was attached to the outlet, so we expected that 40% of each 10-μL aliquot would be water, resulting in a decrease in fluorescein concentration. For the 20-refresh-stroke scheme, the normalized concentration of the dosed wells was approximately 0.6, which is consistent with dilution due to dead volume. For the 10 and 7-refresh-stroke schemes, there was additional dilution because the the infused volume was greater than the volume of drug loaded into the infuse-withdraw line during the drug refresh strokes.

Reducing the relative number of refresh strokes during a drug dose as compared to the number of infuse strokes by changing from the 20-refresh-stroke to the 10-refresh-stroke and 7-refresh-stroke dose schemes resulted in decreases in the output fluorescein concentration, as expected. For the 20-refresh-stroke scheme, the wells immediately following the actively dosed wells had an even higher average fluorescein concentration than that of the dosed wells. This most likely resulted from the refresh stroke volume being larger than the infuse stroke volume, owing to the lower hydrodynamic resistance in the refresh loop path as compared to the infuse-withdraw line. After each cycle of one refresh stroke and one infuse stroke, some additional volume of fluorescein was left in the infuse-withdraw line. By the end of a 20-infuse-stroke dose, these small leftover volumes added up to fill most or all of the infuse-withdraw line, which had a total volume of 10–11 μL. Because the dead volume after the outlet valve was also filled with fluorescein solution, the 20-stroke aliquot deposited into the subsequent well was not diluted by water in the dead volume, and had even higher fluorescence. For the 10-refresh-stroke and 7-refresh-stroke dose schemes, the total infused volume per cycle exceeded the volume of drug loaded into the infuse-withdraw line, so the wells immediately following the actively dosed wells had lower concentrations of fluorescein than the dosed wells, corresponding to leftover fluorescein in the pump being flushed out.

4.4 Acute DNQX Delivery

As we have done in the past,[18,24,26,27] we used DNQX in this study as a test drug because it is a well-known glutamate receptor antagonist that reversibly disrupts hair cell to auditory nerve synaptic transmission when perfused/infused into guinea pig cochlae.[34–36] Our results (Figures 13 and 14) are consistent with previous reports, as infusion of DNQX resulted in suppression of CAP amplitudes and elevation of CAP thresholds, with minimal changes to DPOAEs. After DNQX infusion was stopped, both thresholds and amplitudes returned to near-baseline levels, which is consistent with previous reports on the reversibility of DNQX effects.

We began drug delivery with infusion and withdrawal of AP so that we could switch to DNQX delivery later and demonstrate electronically-controlled dosing. AP perfusion typically results in slight increases in CAP amplitude.[42,43] We observed frequency-dependent decreases in CAP amplitudes during AP infusion, which is consistent with our expectations that there would

be a small amount of DNQX in the AP as an artifact of the pump priming procedure. We roughly estimated the amount of drug left in the infuse-withdraw line after priming with a fluorescein experiment. First we primed the drug reservoir with fluorescein solution, and then we flushed the infuse-withdraw line with 0.5 ml of water. Then we actuated 20 infuse strokes, collected the output in a microwell plate, and measured the fluorescence. Because fluorescein and DNQX are similarly sized molecules, we assumed that they have similar transport characteristics. From this test, we estimate that the concentration of DNQX in the infuse-withdraw line following priming was approximately 60–80 μM. The amplitude changes were small enough that there were no significant threshold elevations. This is consistent with our previous report that CAP amplitudes are more sensitive to DNQX than are thresholds.[26] The amplitudes also recovered slightly during the wait time between infusion and withdrawal, which is consistent with the well-known reversibility of DNQX effects.

During the entire infusion and withdrawal process, there were no changes to DPOAEs, indicating that our pump did not cause any mechanical damage to the inner ear during one full cycle of reciprocating delivery. After reciprocating AP delivery was complete, we initiated the DNQX delivery program, which resulted in CAP amplitude suppression and increased CAP thresholds after a short delay (about 15 minutes) due to the time it took for the device to clear AP from the dead volume at the outlet. This demonstrated our ability to electronically control drug dosing in an animal model using our device.

We used the frequency-dependent changes in CAPs and our knowledge of the well-known tonotopic organization of the cochlea[44] to infer the distribution and spreading of DNQX over time during drug delivery. We estimated that the end of the cannula was positioned in the 12–16 kHz region of the cochlea, which is consistent with our CAP data showing the largest and earliest DNQX effects at 16 kHz (Figures 13, 14, and 15). The cochleostomy, located approximately in the 28 kHz region, was near the cochlear aqueduct.[45] We expected the drug to flow from the cannula basally toward the cochlear aqueduct, resulting in fast distribution of DNQX to basal frequency regions (above 16 kHz), and slower distribution of of DNQX to apical frequency regions (below 12 kHz), where transport of DNQX was expected to be primarily diffusive. Based on our previous data,[26] we did not expect DNQX to reach frequency regions below 8 kHz within the delivery time frame explored in this study, so we did not monitor CAPs at those frequencies during delivery. However, we measured CAPs at 5.6, 4, and 2.78 kHz starting immediately after the end of DNQX delivery and hourly thereafter, and did not observe any amplitude changes or threshold elevations at those frequencies. CAP suppression at 8 kHz was delayed and smaller in magnitude than at more basal frequencies, which is also consistent with slower apical transport. At 24 and 32 kHz, the maximum drug effects were observed at the same time as they were for 16 kHz, indicating fast, convective delivery. However, there was less CAP suppression at 24 and 32 kHz than at 16 or 12 kHz.

For the experiments discussed here, we chose an arbitrary wait time between infusion of AP and withdrawal of AP because we did not expect the AP to significantly affect hearing. For reciprocating delivery of a drug, however, this wait time should be optimized for maximum delivery efficiency. The wait time should not be too short, because infused drug will not have time to diffuse throughout the cochlea. If the wait time is too long and the effects of the drug are reversible, as is the case for DNQX, the animal may fully recover from the effects of the drug before the next dose is delivered. By shutting off the pump after DNQX delivery and observing recovery, we have generated data that suggests that 1 hour will be an appropriate wait time between infusion and withdrawal for reciprocating delivery of DNQX.

5 Conclusions

We designed, characterized, and acutely tested a reciprocating micropump for intracochlear drug delivery. The device has integrated drug storage and is capable of electronically-controlled dosing. We designed the micropump to be part of a head-mounted system for inner-ear drug delivery experiments in guinea pig animal models, enabling long-term pharmacokinetic characterization of new drugs. With these long-term experiments in mind, we included features in our microfluidics that help reduce power consumption such as fluidic capacitors; this will be critical for future chronic experiments in which the pump will be powered by a portable battery. We also paid special attention to reducing outlet dead volume to increase the efficiency of reciprocating delivery, and to minimizing peak flow rates for safety.

We showed that our micropump is robust enough to perform well when hydrodynamic resistance is added to the outlet, enabling it to maintain drug delivery against pressures 50 times greater than the typical intracochlear pressure in guinea pigs. When we used fluorescein solution as a test drug, we showed that delivery of drug doses can be controlled electronically, including switching between fluorescein and water delivery, and reducing the effective concentration of fluorescein delivered. We demonstrated safe, efficacious drug delivery and electronically controlled dosing in guinea pigs by using the glutamate receptor antagonist, DNQX, as a test drug. Reciprocating delivery of AP did not result in hearing threshold elevations, but electronically switching from AP to DNQX delivery resulted in frequency-dependent CAP amplitude suppresssion and threshold elevations that were consistent with the expected transport path of the drug and guinea pig cochelar anatomy. There were no changes to DPOAEs throughout delivery of AP and DNQX, indicating that our pump did not cause any mechanical damage acutely.

When paired with miniaturized electronic control hardware

and integrated into a head-mount enclosure, our micropump will enable highly controlled, chronic drug delivery experiments in animal models and minimize systemic exposure to the drug. The increased dosage precision afforded by delivery via cochleostomy using our micropump will facilitate characterization of pharmacokinetics in drug development experiments. Reducing systemic exposure will likely be critical when hearing-restoring drugs are used for treatment in humans as well, as many existing drugs and early drug candidates are toxic when delivered systemically. The electronically-controlled dosing demonstrated in this study can also be adapted for sequential delivery of a timed series of drugs, which will likely be important for hair-cell regeneration therapy.

Acknowledgments

This work was supported by NIH NIDCD Grant 5 R01 DC006848-08.

References

1 S. K. Juhn and L. P. Rybak, *Acta Otolaryngol.*, 2008, **91**, 529–534.

2 S. K. Juhn, B. A. Hunter and R. M. Odland, *Int. Tinnitus J.*, 2001, **7**, 72–83.

3 D. S. Haynes, M. O'Malley, S. Cohen, K. Watford and R. F. Labadie, *Laryngoscope*, 2007, **117**, 3–15.

4 K. Mizutari, M. Fujioka, M. Hosoya, N. Bramhall, H. J. Okano, H. Okano and A. S. B. Edge, *Neuron*, 2013, **77**, 58–69.

5 W. S. Kang, S. Sun, K. Nguyen, B. Kashemirov, C. E. Mckenna, S. A. Hacking, A. M. Quesnel, W. F. Sewell, M. J. Mckenna and D. H. Jung, *Otol. Neurotol.*, 2015, **36**, 953–960.

6 K. J. Doyle, C. Bauch, R. Battista, C. Beatty, G. B. Hughes, J. Mason, J. Maw and F. L. Musiek, *Otol. Neurotol.*, 2004, **25**, 1034–1039.

7 A. N. Salt and S. K. R. Plontke, *Drug Discov. Today*, 2005, **10**, 1299–1306.

8 R. T. Richardson, A. Wise, S. O'Leary, J. Hardman, D. Casley and G. Clark, *Hear. Res.*, 2004, **198**, 25–35.

9 R. T. Richardson, F. Noushi and S. O'Leary, *Audiol. Neurotol.*, 2006, **11**, 343–356.

10 R. T. Richardson, A. K. Wise, B. C. Thompson, B. O. Flynn, P. J. Atkinson, N. J. Fretwell, J. B. Fallon, G. G. Wallace, R. K. Shepherd, G. M. Clark and S. J. O'Leary, *Biomaterials*, 2009, **30**, 2614–2624.

11 L. M. Bianchi and Y. Raz, *Curr. Drug Targets. CNS Neurol. Disord.*, 2004, **3**, 195–199.

12 Y. Maeda, A. M. Sheffield and R. J. H. Smith, *Hear. Res.*, 2010, **242**, 1–21.

13 J. Defourny, S. Mateo Sánchez, L. Schoonaert, W. Robberecht, A. Davy, L. Nguyen and B. Malgrange, *Nat. Commun.*, 2015, **6**, 7017.

14 M. Praetorius, K. Baker, D. E. Brough, P. Plinkert and H. Staecker, *Hear. Res.*, 2007, **227**, 53–58.

15 M. Igarashi, K. Ohashi and M. Ishii, *Acta Otolaryngol.*, 1986, **101**, 161–164.

16 R. A. Buckingham and G. E. Valvassori, *Ann. Otol. Rhinol. Laryngol.*, 2001, **110**, 113–7.

17 M. Thorne, A. N. Salt, J. E. DeMott, M. M. Henson, O. W. Henson and S. L. Gewalt, *Laryngoscope*, 1999, **109**, 1661–1668.

18 E. E. L. Pararas, Z. Chen, J. Fiering, M. J. Mescher, E. S. Kim, M. J. McKenna, S. G. Kujawa, J. T. Borenstein and W. F. Sewell, *J. Control. Release*, 2011, **152**, 270–277.

19 A. Fridberger, J. T. van Maarseveen, E. Scarfone, M. Ulfendahl, B. Flock and A. Flock, *Acta Physiol. Scand.*, 1997, **161**, 239–252.

20 O. Handzel, H. Wang, J. Fiering, J. T. Borenstein, M. J. Mescher, E. E. Leary Swan, B. A. Murphy, Z. Chen, M. Peppi, W. F. Sewell, S. G. Kujawa and M. J. McKenna, *Audiol. Neurotol.*, 2009, **14**, 308–314.

21 W. F. Sewell, J. T. Borenstein, Z. Chen, J. Fiering, O. Handzel, M. Holmboe, E. S. Kim, S. G. Kujawa, M. J. McKenna, M. M. Mescher, B. Murphy, E. E. Eary Swan, M. Peppi and S. Tao, *Audiol. Neurotol.*, 2009, **14**, 411–422.

22 E. E. L. Swan, M. J. Mescher, W. F. Sewell, S. L. Tao and J. T. Borenstein, *Adv. Drug Deliv. Rev.*, 2008, **60**, 1583–1599.

23 S. K. Plontke, H. Löwenheim, J. Mertens, C. Engel, C. Meisner, A. Weidner, R. Zimmermann, S. Preyer, A. Koitschev and H.-P. Zenner, *Laryngoscope*, 2009, **119**, 359–369.

24 E. S. Kim, E. Gustenhoven, M. J. Mescher, E. E. L. Pararas, K. A. Smith, A. J. Spencer, V. Tandon, J. T. Borenstein and J. Fiering, *Lab Chip*, 2014, **14**, 710–21.

25 J. Fiering, M. J. Mescher, E. E. Leary Swan, M. E. Holmboe, B. A. Murphy, Z. Chen, M. Peppi, W. F. Sewell, M. J. McKenna, S. G. Kujawa and J. T. Borenstein, *Biomed. Microdevices*, 2009, **11**, 571–578.

26 V. Tandon, W. S. Kang, A. J. Spencer, E. S. Kim, E. E. L. Pararas, M. J. McKenna, S. G. Kujawa, M. J. Mescher, J. Fiering, W. F. Sewell and J. T. Borenstein, *Biomed. Microdevices*, 2015, **17**, 3–21.

27 Z. Chen, S. G. Kujawa, M. J. McKenna, J. O. Fiering, M. J. Mescher, J. T. Borenstein, E. E. Leary Swan and W. F. Sewell, *J. Control. Release*, 2005, **110**, 1–19.

28 http://www.who.int/topics/deafness/en/.

29 B. S. Wilson and M. F. Dorman, *Hear. Res.*, 2008, **242**, 3–21.

30 M. C. Holley, *Drug Discov. Today*, 2005, **10**, 1269–1282.

31 G. S. G. Géléoc and J. R. Holt, *Science*, 2014, **344**, 1241062.

32 U. Müller and P. G. Barr-Gillespie, *Nat. Rev. Drug Discov.*, 2015, **242**, 3–21.

33 M. J. Mescher, E. E. L. Swan, J. Fiering, M. Holmboe, W. F.

Sewell, S. G. Kujawa, M. J. McKenna and J. T. Borenstein, *J. Microelectromechanical Syst.*, 2009, **18**, 501–510.
34 T. Littman, R. P. Bobbin, M. Fallon and J. L. Puel, *Hear. Res.*, 1989, **40**, 45–53.
35 B. W. Agranoff, *Fed. Proc.*, 1975, **34**, 1911–1914.
36 T. N. Parks, *Hear. Res.*, 2000, **147**, 77–91.
37 M. Yoshida and L. D. Lowry, *Am. J. Otolaryngol.*, 1984, **5**, 159–65.
38 A. Böhmer and J. C. Andrews, *Arch. Otorhinolaryngol.*, 1989, **246**, 65–66.
39 J. C. Andrews, a. Böhmer and L. F. Hoffman, *Laryngoscope*, 1991, **101**, 661–668.
40 A. Böhmer, *Laryngoscope*, 1991, **101**, 1307–1312.
41 E. O. Thalen, H. P. Wit, J. M. Segenhout and F. W. Albers, *Acta Otolaryngol.*, 2001, **121**, 470–476.
42 S. E. Barron, R. P. Bobbin, P. Guth and C. Norris, *Hear. Res.*, 1987, **31**, 147–153.
43 R. P. Bobbin and G. Ceasar, *Hear. Res.*, 1987, **25**, 77–81.
44 D. D. Greenwood, *Hear. Res.*, 1996, **94**, 157–162.
45 A. F. Ghiz, A. N. Salt, J. E. DeMott, M. M. Henson, O. W. Henson and S. L. Gewalt, *Hear. Res.*, 2001, **162**, 105–112.